Materials Chemistry and Physics 141 (2013) 324–332

Contents lists available at SciVerse ScienceDirect

Materials Chemistry and Physics

journal homepage: www.elsevier.com/locate/matchemphys

Block copolymer assisted self-assembly of nanoparticles into Langmuir–Blodgett films: Effect of polymer concentration

Beatriz Martín-García, M. Mercedes Velázquez*

Departamento de Química Física, Facultad de Ciencias Químicas, Universidad de Salamanca, E-37008 Salamanca, Spain

HIGHLIGHTS

- Effect of the surface composition on the LB films architecture.
- QDs/polymer LB films morphology interpreted in terms of dewetting mechanism.
- The dewetting mechanism depends on the Langmuir monolayer state.

GRAPHICAL ABSTRACT

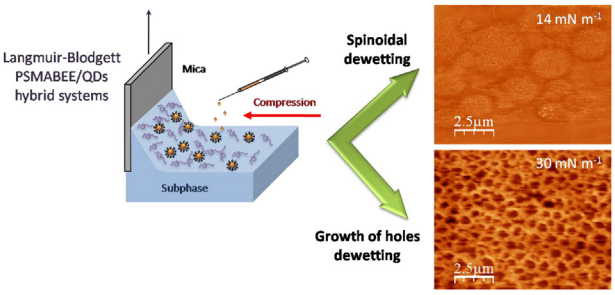

ARTICLE INFO

Article history:
Received 12 December 2012
Received in revised form
18 March 2013
Accepted 2 May 2013

Keywords:
Polymers
Thin Films
Nanostructures
Atomic Force Microscopy (AFM)
Electron microscopy (STEM, TEM and SEM)

ABSTRACT

We propose to use the self-assembly ability of a block copolymer to obtain CdSe quantum dots (QDs) structures of different morphology. The methodology proposed consist in transferring mixed Langmuir monolayers of QDs and the polymer poly (styrene-co-maleic anhydride) partial 2 buthoxy ethyl ester cumene terminated, PS-MA-BEE onto mica by the Langmuir–Blodgett (LB) methodology. The morphology of the LB films was analyzed by AFM and TEM measurements. Our results show that it is possible to modulate the self-assembly process by modifying the composition of the mixed Langmuir monolayer precursor of the LB film. The different morphologies are interpreted according to two different dewetting mechanisms, growth of holes and spinodal-like dewetting. The growth of holes dewetting process is driven by gravitatory effects and was observed for LB films obtained by transferring Langmuir monolayer of the smallest elasticity values in which the polymer is in brush conformation. The spinodal dewetting mechanism prevailed when the Langmuir monolayer presents the highest elasticity values.

1. Introduction

The nanoparticle–polymer blend systems have attracted much interest in the last years due to its numerous potential applications. In particular, nanocomposites prepared with polymers and inorganic fillers, in which the inorganic component has at least one dimension below 100 nm, have been proposed to achieve significant enhancements in material properties [1]. However, many nanofillers used in nanocomposites tend to agglomerate by attractive interactions [2,3] decreasing the quality of nanocomposites. Therefore, the most recent efforts involve the use of polymer or surfactant molecules to minimize filler agglomeration. Despite the great interest aroused in the last years, more work must be carried out to develop multifunctional materials with novel electric, magnetic or optical properties [4–7].

An important issue concerning the properties of filler deposited on solids is to achieve control over the organization and assembly of nanoparticles at interfaces. Many techniques have been used to

* Corresponding author. Departamento de Química Física, Universidad de Salamanca, Facultad de Ciencias Químicas, Plaza de los Caídos s/n, 37008 Salamanca, Spain. Fax: +34 923 294574.
E-mail address: mvsal@usal.es (M.M. Velázquez).

0254-0584/$ – see front matter © 2013 Elsevier B.V. All rights reserved.
http://dx.doi.org/10.1016/j.matchemphys.2013.05.017

achieve good-quality nanocomposites [8–10]. A common methodology employs templates to control the deposition during solvent evaporation. However, template fabrication usually involves lithography processes, which are often limited by the special equipment required. The Langmuir–Blodgett methodology (LB) has been proposed as a platform that renders the self-assembly process of different nanomaterials at the air–water interface under well controlled and reproducible conditions [11–14]. Therefore, it offers the possibility of preparing polymers and nanoparticles reproducible films with the control of the interparticle distance necessary to exploit the nanocomposites in technological applications.

In previous work [12] we used the LB methodology to obtain CdSe QDs self-assemblies by transferring onto mica mixed Langmuir monolayers of QDs and the polymer poly (octadecene-co-maleic anhydride), (PMAO); and QDs and the Gemini surfactant ethyl-bis(dimethyl octadecylammonium bromide). Our results showed that it is possible to modulate the architecture of QDs self-assemblies by modifying the composition of the Langmuir monolayers precursors of LB films. Thus, mixed PMAO/QDs films are constituted by hexagonal networks in which QDs are adsorbed on rims, while Gemini/QDs LB films are formed by arrays of droplets. The different architectures were attributed to distinct dewetting processes, nucleation and growth of holes for PMAO/QDs, and spinodal dewetting for Gemini/QDs films. Taking into account that the growth of holes dewetting mechanism is driven by the gravitational effect and the capillary waves address the spinodal one, the predominance of one mechanism depends on a subtle balance between the molecular weight and the surface properties of the film components [15].

In order to evaluate the role of the surface properties of the Langmuir monolayer precursor of the LB film on the dewetting mechanism, we have enlarged our previous study to the block copolymer, poly (styrene-co-maleic anhydride) partial 2 buthoxy ethyl ester cumene terminated, PS-MA-BEE. In the current work we use the polymer PS-MA-BEE as matrix of QDs for preparing mixed LB films at different polymer composition. We choose this polymer because it aggregates at the interface at a given polymer concentration [14]. Thus, as the polymer aggregation modifies the film surface properties [16–20], it provides us an excellent way to study the effect of the surface properties on the dewetting mechanism. With this objective in mind, we have studied the surface properties of PS-MA-BEE/QDs mixed Langmuir monolayers with different composition. The characterization of these mixed monolayers allows us to select monolayers with very different surface properties and to transfer them onto mica, in order to investigate the role of these properties on both, the morphology of QDs films and the dewetting mechanism. Moreover, styrene/maleic anhydride copolymers have shown potential application in optical waveguides, electron beam resists and photodiodes [21,22]. Therefore, it could be a good candidate to prepare hybrid materials for optoelectronic devices fabrication [23–25].

2. Experimental section

2.1. Materials

Trioctylphosphine (TOP, technical grade, 90%), cadmium oxide powder (99.99%), selenium powder (99.99%), oleic acid (technical grade, 90%) and 1-octadecene were purchased from Sigma–Aldrich. The polymer poly (styrene-co-maleic anhydride) partial 2 buthoxy ethyl ester cumene terminated, PS-MA-BEE hereafter, was supplied from Sigma–Aldrich, Scheme 1. The ester:acid ratio 1:1 and the polymer molecular weight M_n = 2.5 kDa were provided by the manufacturer. The materials were used as received without further purification. Chloroform (PAI, filtered) used to prepare the spreading solutions was from Sigma–Aldrich. The concentrations range for the components in the spreading solutions were from 1.25×10^{-7} to 6.3×10^{-7} M and 0.060 to 0.0002 mg mL^{-1} for QDs and PS-MA-BEE, respectively, depending on the mixture mole ratio. The water used as subphase was ultra purified by using a combination of RiOs and Milli-Q systems from Millipore. The LB substrate muscovite (mica) quality V-1 was supplied by EMS (USA). The mica surface was freshly cleaved before use.

The hydrophobic CdSe QDs were synthesized by the method proposed by Yu and Peng [26]. QDs were collected as powder by size-selective precipitation with acetone and dried under vacuum. The diameter of the QDs (3.55 ± 0.05 nm) was determined by the position of the maximum of the visible spectrum of the QDs dispersed in chloroform [27]. The concentration of nanocrystals was calculated from the UV–Vis absorption spectrum of the QDs solutions by using the extinction coefficient per mole of nanocrystals at the first excitonic absorption peak [27]. UV–Vis absorption spectra were recorded on a Shimadzu UV-2401PC spectrometer.

2.2. Langmuir and Langmuir–Blodgett experiments

The surface pressure isotherms were recorded on a Langmuir Mini-trough (KSV, Finland) placed in an anti-vibration table. The Langmuir–Blodgett deposition was carried out with a KSV2000 System 2 from KSV. Monolayers were transferred by symmetric barrier compression (5 mm min^{-1}) with the substrate into the trough by vertically dipping it up at 5 mm min^{-1}. Spreading solution was deposited onto the water subphase with a Hamilton microsyringe. The syringe precision was 1 μL. The surface pressure was measured with a Pt-Wilhelmy plate connected to an electrobalance. The subphase temperature was maintained at (23.0 ± 0.1) °C by flowing thermostated water through jackets at the bottom of the trough. The temperature near the surface was measured with a calibrated sensor from KSV. The water temperature was controlled by means of a thermostat/cryostat Lauda Ecoline RE-106.

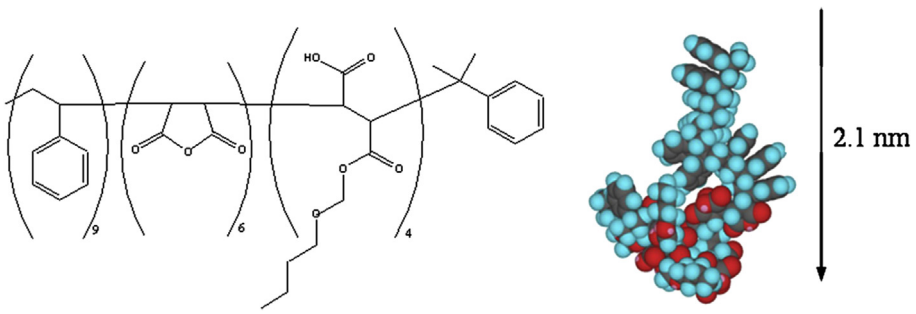

Scheme 1. Molecular structure of poly (styrene-co-maleic anhydride) partial 2-buthoxy ethyl ester cumene terminated and the optimum conformation calculated within the MM2 approximation.

2.3. Brewster Angle Microscopy (BAM)

The Langmuir monolayers were visualized with a Brewster Angle Microscope Optrel BAM 3000 from KSV equipped with a Helium–Neon laser of 10 mW (632.8 nm) which is reflected off the air–water interface at approximately 53.15°, Brewster Angle. The microscope is also equipped with a digital camera model Kam Pro-02 (768 × 494 pixels) from EHD and an objective Mitutoyo (5×).

2.4. Atomic Force Microscopy (AFM)

AFM images of the LB films deposited onto freshly cleaved mica were obtained in constant repulsive force mode by AFM (Nanotec Dulcinea, Spain) with a rectangular microfabricated silicon nitride cantilever (Olympus OMCL-RC800PSA) with a height of 100 μm, a Si pyramidal tip and a spring constant of 0.73 mN m^{-1}. The scanning frequencies were usually in the range of 0.5 and 1.2 Hz per line. The measurements were carried out under ambient laboratory conditions with the WSXM 5.0 program [28].

2.5. Transmission Electron Microscopy (TEM)

TEM images of the LB films deposited on Formvar®–carbon coated copper grids were taken with 80 kV TEM (ZEISS EM 902, Germany). The LB deposition onto copper grids was realized at a speed up of 1 mm min^{-1}.

3. Results and discussion

3.1. Langmuir monolayers for mixed QD/polymer systems

Prior to the LB deposition we have studied the surface properties of the Langmuir monolayers by recording the surface pressure–concentration isotherms of the pure components and mixtures of QDs and polymer at different composition. Fig. 1a shows the isotherms of QDs and PS-MA-BEE. The isotherms agree very well with those reported previously [14,29].

In the case of mixed monolayers it is well established that their surface properties depend on the spreading technique [30,31]; therefore we test the isotherm properties of monolayers obtained by spreading both components at the interface, named as co-spreading, or adding the components separately. In all cases the isotherms were very stable. A representative example for mixed monolayers of polymer mole fraction $X_P = 0.39$ is presented in Fig. 1b. Significant differences between the isotherms can be observed. Thus, from the three spreading procedures the densest monolayer is that obtained by co-spreading. This behavior was observed in other systems [30,31] and ascribed to the existence of attractive interactions between polymer and QDs molecules in the spreading solution [31]. As demonstrated in our previous work [12,30], the co-spreading method proved to be the most reproducible technique and consequently, was chosen to build the mixed QDs/PS-MA-BEE monolayers.

Fig. 1a also presents the isotherms of mixed monolayers of QDs and the polymer PS-MA-BEE with different composition. As can be seen the isotherms of the polymer PS-MA-BEE and mixed with QDs at high polymer concentration, $X_P \geq 0.93$, present a plateau at the surface pressure value of 30 mN m^{-1}. This plateau could be related with phase coexistence and has been previously observed in other block–copolymer isotherms [32–34]. To gain insight into the states of the monolayers we have calculated the equilibrium elasticity modulus, ε_0, from the surface pressure isotherms and: $\varepsilon_0 = \Gamma(\delta\Pi/\delta\Gamma)$. For the sake of comparison the elasticity values are represented against the surface pressure values in Fig. 1c. Our results presented in Fig. 1c show that the monolayer elasticity increases with the surface pressure and reaches a maximum at a given surface pressure. The maximum position is shifted to higher surface pressures for mixed monolayers. Beyond the maximum, when the surface pressure is further increased, the elasticity decreases and for monolayers with surface compositions $X_P \geq 0.93$ the elasticity goes through a minimum at the surface pressure value of 30 mN m^{-1}. The region around the elasticity minimum corresponds to the plateau in the surface pressure isotherm. For comparative purposes dashed lines in Fig. 1c delimit the plateau region.

Comparison between the elasticity and surface pressure isotherms of PS-MA-BEE with those reported for other Langmuir monolayers of block copolymers allowed us to obtain information about the polymer states at the interface. Results in the literature demonstrated that at low surface pressures the polymer blocks presents an almost flat conformation without tails protruding into the subphase, in this regime the elasticity increases with the surface concentration until it reaches the maximum value. In this state the monolayer can be formed by aggregates with different features [32–34]. As it is discussed next, the polymer PS-MA-BEE aggregates in stripes. At surface pressures beyond the elasticity maximum, the polymer hydrophilic blocks protrude into the water subphase and the elasticity values decrease until a minimum in which the polymer brush conformation predominates. In this region the aggregates coexist with brush structures, and it corresponds to the plateau in the surface pressure isotherms. In our system the phase coexistence is between stripes and brushes. For surface pressures beyond the elasticity minimum, is generally admitted that interactions between the polymer blocks lead to a further increase of the surface elasticity [35,36].

For mixed polymer/QDs monolayers, the morphology of the elasticity curves, Fig. 1c, also depends on the surface composition. From results in Fig. 1c, it is possible to notice that the minimum in the elasticity curve appears for mixed monolayers with high polymer concentration, $X_P \geq 0.93$. Taking into account that the elasticity minimum was ascribed to the polymer brush state, the behavior observed in mixtures seems to indicate that the brush regime is only reached in mixed monolayers with high polymer concentration.

To gain insight into the morphology of PS-MA-BEE/QDs monolayers, we use the Brewster Angle Microscopy (BAM). Several images corresponding to monolayers at two surface pressure values, 14 mN m^{-1} and 30 mN m^{-1} and different surface compositions are collected in Fig. 2. BAM images of monolayers at 14 mN m^{-1} and low polymer concentration, Fig. 2a and b, shows QD agglomerates. However, when the polymer concentration increases, the QD agglomeration decreases, Fig. 2c and d. This behavior can be interpreted if one considers that in the absence or at low polymer concentration the interactions between water subphase and the QDs stabilizer, TOPO, are too weak, and they promote the agglomeration of nanoparticles at the air–water interface [2,37]. However, when the polymer concentration increases, attractive interactions between the polymer hydrophobic block and the alkyl chains of TOPO favor the QDs spreading on the water surface across the polymer hydrophilic blocks avoiding the QDs agglomeration [29,38,39].

Monolayers with high surface coverage ($\pi = 30$ mN m^{-1}) are constituted by domains so close-packed that BAM images do not allow us to visualize details of its morphology. As illustrative example, we present in Fig. 2e the BAM image of the mixed monolayer at 30 mN m^{-1} and $X_P = 0.94$.

3.2. Langmuir–Blodgett films of pure components

The next step was to transfer the polymer Langmuir monolayers from the air–water interface onto mica by using the Langmuir–

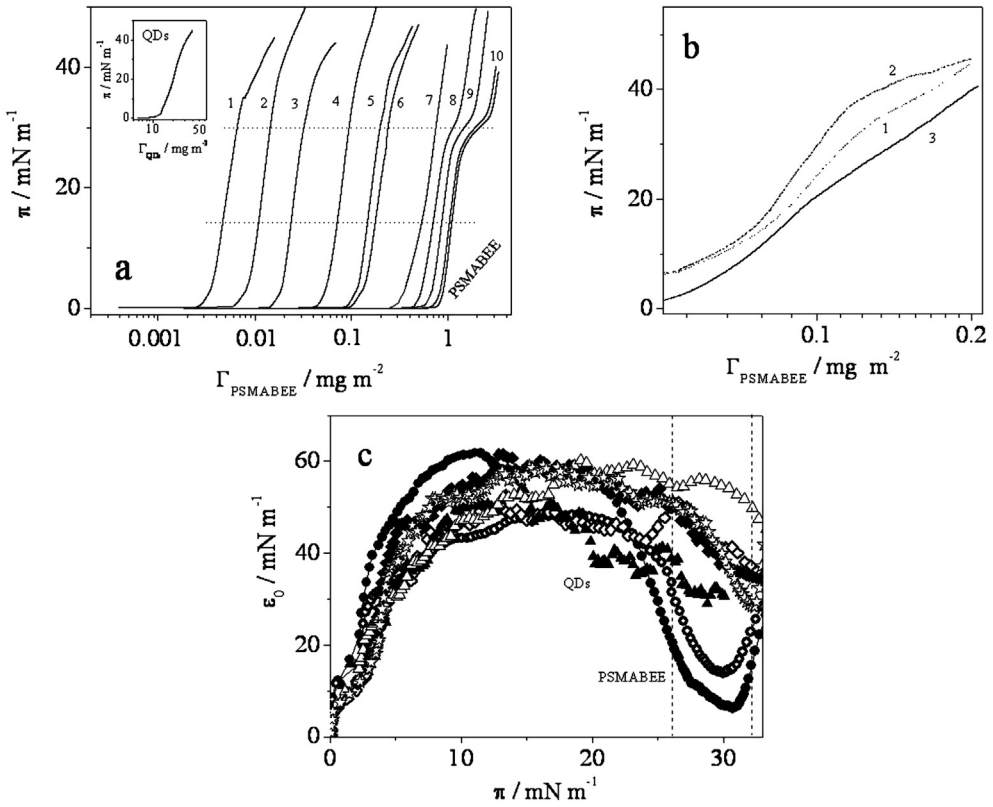

Fig. 1. (a) Surface pressure isotherms of mixed Langmuir monolayers of QDs and PS-MA-BEE with polymer mole fraction of: 0.05 (1); 0.10 (2); 0.25 (3); 0.43 (4); 0.54 (5); 0.72 (6); 0.89 (7); 0.94 (8); 0.97 (9); 0.98 (10) and pure PS-MA-BEE. The inset shows the QDs surface pressure isotherm. The dotted lines indicate the surface pressures for the LB deposition: 14 and 30 mN m^{-1}. (b) Surface pressure isotherms for QDs/PS-MA-BEE mixed monolayers at polymer mole fraction of 0.39 obtained with separate spreading of QDs and PS-MA-BEE (1) and PS-MA-BEE and QDs (2), respectively, and co-spreading (3). (c) Equilibrium surface elasticity vs. surface pressure for several mixed Langmuir monolayers of QDs and PS-MA-BEE at different polymer mole fraction: QDs (closed triangles); 0.05 (open rhombi); 0.25 (closed rhombi); 0.43 (open triangles); 0.54 (stars); 0.94 (open circles); and PS-MA-BEE (closed circles). The dashed lines delimit the surface pressures where the plateaux in the surface pressure isotherms appear.

Blodgett technique. The monolayers were transferred at the surface pressure values of 14 and 30 mN m^{-1}, respectively. We chose these monolayers because they correspond to representative states of the polymer monolayer. Thus, the monolayer at the surface pressure of 14 mN m^{-1} is far from the brush regime and corresponds to the most elastic surface state, while the monolayer at 30 mN m^{-1} corresponds to the polymer brush regime, minimum in the elasticity curve. For the sake of comparison, we have also transferred QDs monolayers at the same surface pressure values, 14 and 30 mN m^{-1}, respectively.

The AFM images of QDs films are collected in Fig. 3a and b. As can be seen in Fig. 3a the QDs film is mainly constituted by QDs

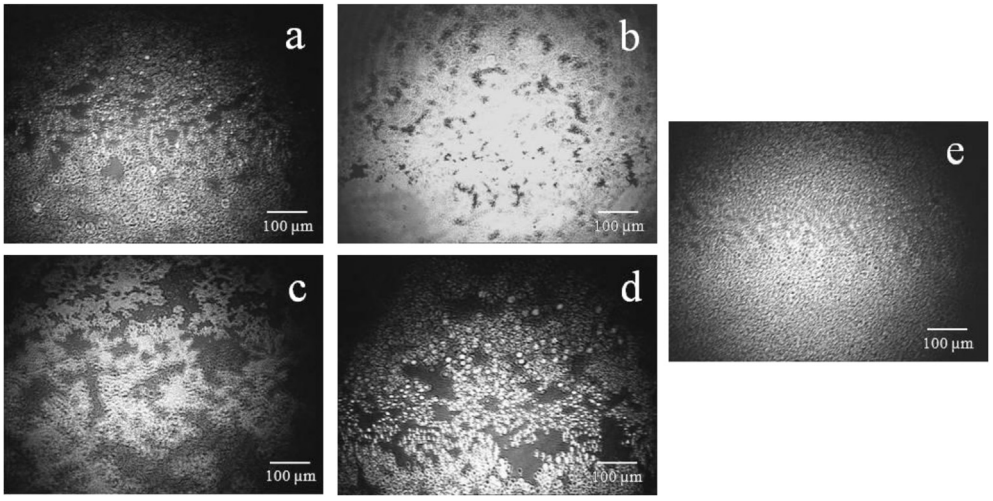

Fig. 2. BAM images (800 × 600 μm) at 14 mN m^{-1} for different QDs/PS-MA-BEE mixed monolayers with different polymer mole fractions: (a) pure QDs; (b) 0.39; (c) 0.94 and (d) 0.97. BAM image of QDs/PS-MA-BEE mixed monolayer at 30 mN m^{-1} and at polymer mole fraction of 0.94 (e).

agglomerates of different sizes and when the surface concentration of the QDs transferred was further increased until a surface pressure value of 30 mN m^{-1}, the density of agglomerates increases and even 3D aggregates are formed. This fact can be interpreted if one considers that due to the low affinity of the QDs stabilizer TOPO and the solid mica, the nanoparticle spreading is too weak. This fact favors the QD agglomeration.

On the other hand, the AFM images of polymer LB films, Fig. 3c and d, revealed that the films obtained at different surface densities have different morphologies. Thus, the polymer aggregates in stripes of roughness ~10 nm when the surface pressure of the Langmuir monolayer transferred on mica is 14 mN m^{-1}, Fig. 3c [14], while films with domains separated by holes were observed when the surface coverage increases until 30 mN m^{-1}, Fig. 3d. The domain

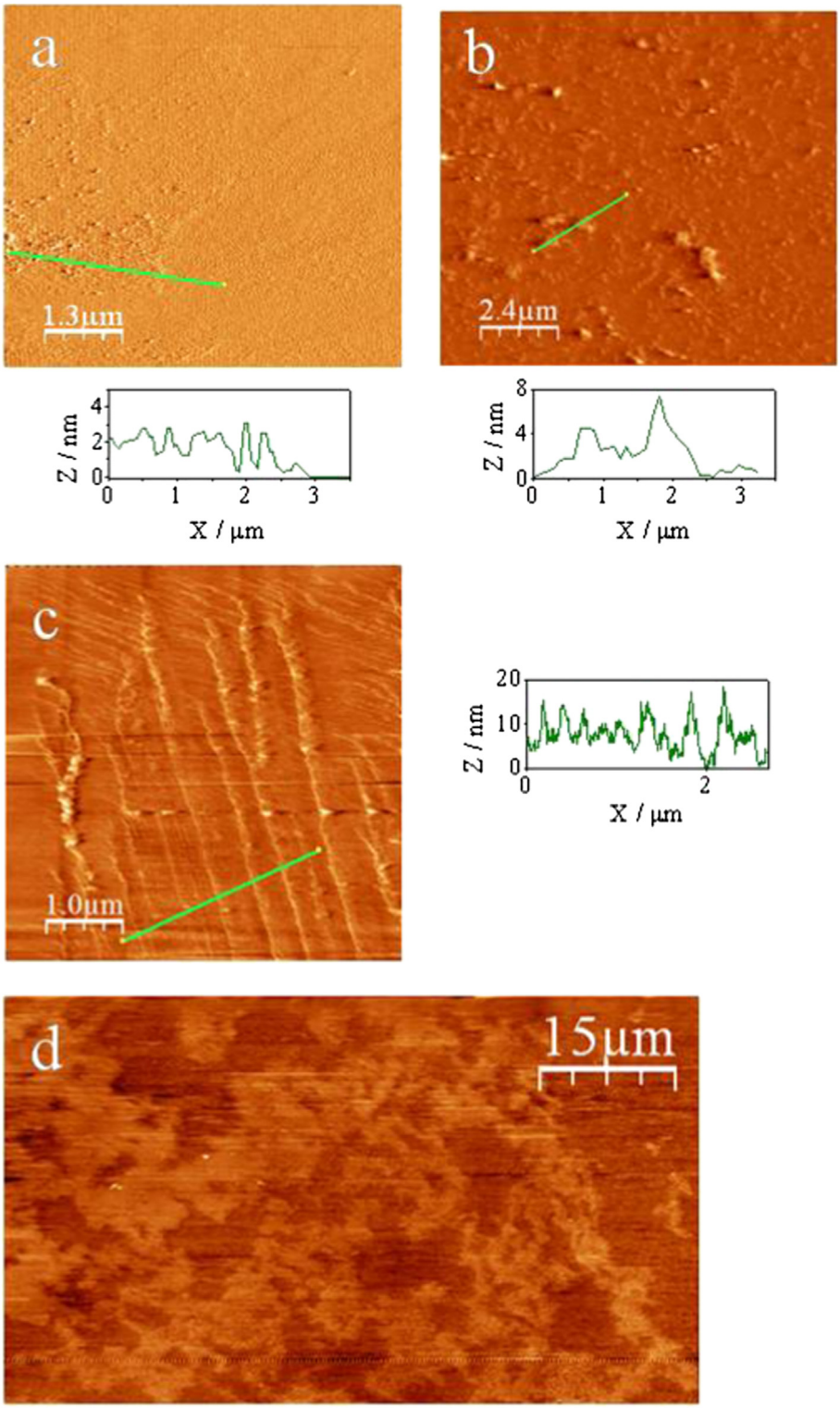

Fig. 3. AFM images of QDs (a, b) and PS-MA-BEE (c, d) LB films deposited at the surface pressures values of (a, c) 14 mN m^{-1} and (b, d) 30 mN m^{-1}.

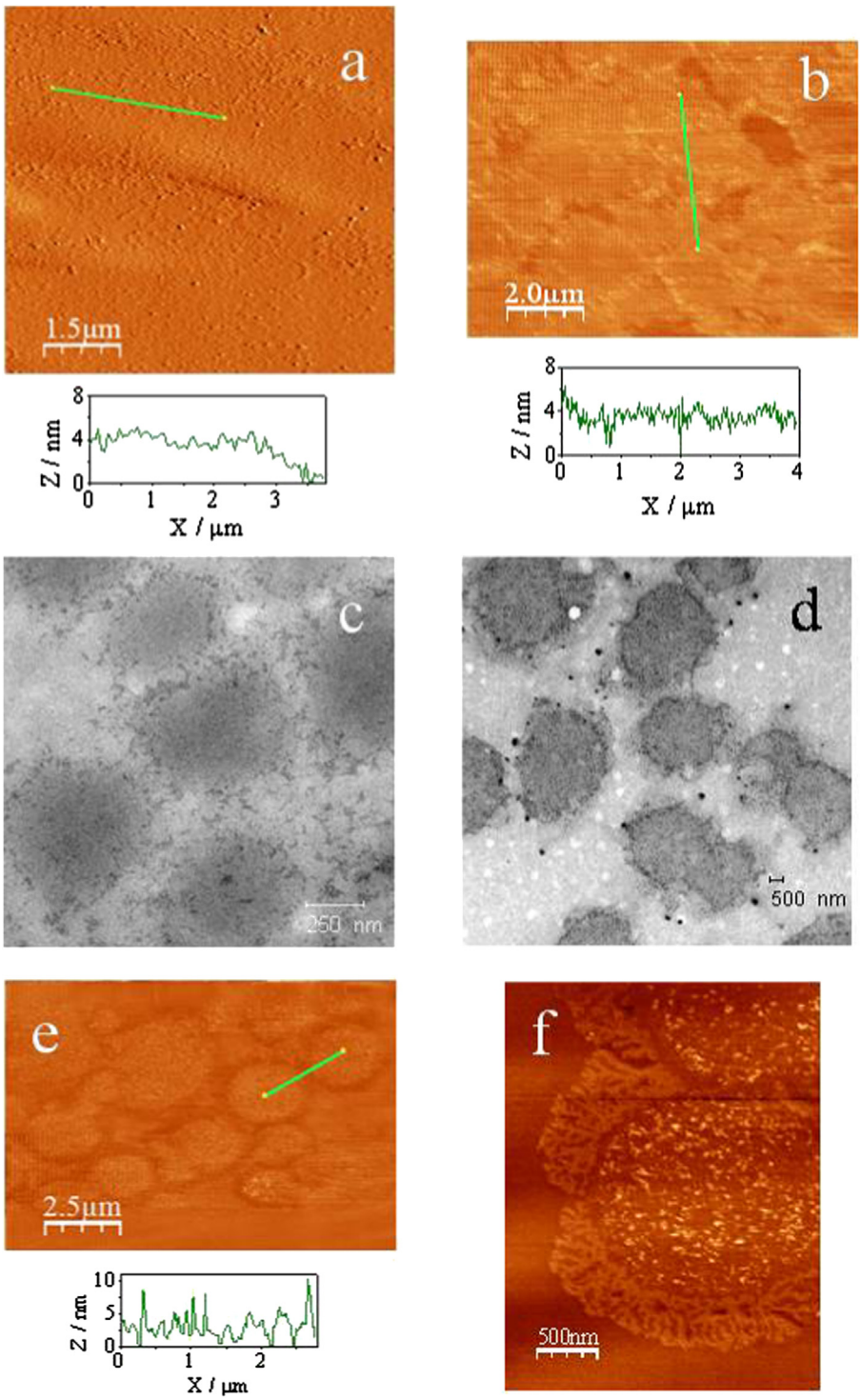

Fig. 4. AFM (a, b, e, f) and TEM (c, d) images of mixed QDs/PS-MA-BEE LB films the surface pressure of 14 mN m^{-1}. The film composition expressed as polymer mole fraction is: 0.25 (a); 0.39 (b); 0.54 (c) and 0.97 (d, e, f).

roughness found was ~2 nm, which agrees with the polymer thickness calculated by means of molecular mechanic MM2 calculations (2.1 nm).

In polymer LB films the existence of two different features depending on the polymer concentration points to two distinct dewetting mechanisms. Thus, stripes and other 2D structures were previously observed and interpreted by spinodal dewetting mechanism [40–42]. Conversely, domains separated by holes were observed in films in which the gravitatory effects are important [15]. In an attempt to interpret the different behavior observed it was necessary to analyze the driving forces involved in the surface arrangement. Taking into account that the molecular weight of our polymer is too low, one expects that the gravitatory effects were neglected; however, it is necessary to compare this effect with that of the capillary waves. It is well established that the damping coefficient passes though a maximum at low elasticity values [43] and

decreases when the elasticity modulus increases. Accordingly, in the case of the most elastic monolayer (π = 14 mN m^{-1}), the capillary effects could predominate against the gravitatory ones and the dewetting mechanism is driven by the capillary waves resulting in films constituted by stripes. Conversely, in less elastic monolayer (π = 30 mN m^{-1}), the capillary waves are quickly damped and the polymer film breaks in domains separated by holes due to gravitatory effects. Consequently, the growth of holes dewetting mechanism predominates against the capillary one in this monolayer state.

Table 1
Average values of the feature dimensions of QDs/PS-MA-BEE mixed LB films obtained from AFM measurements.

X_P	Domains (dots) at π = 14 mN m^{-1}		X_P	Holes at π = 30 mN m^{-1}	
	X-direction/μm	*Y*-direction/μm		*X*-direction/μm	*Y*-direction/μm
0.54	2.22 ± 1.36	2.15 ± 1.29	0.93	0.83 ± 0.19	0.77 ± 0.20
0.94	1.14 ± 0.39	1.05 ± 0.31	0.94	0.57 ± 0.18	0.47 ± 0.16
0.98	0.50 ± 0.23	0.54 ± 0.23			

Reported values are averages and error represents the standard deviation determined from at least 50 surface features.

3.3. Langmuir–Blodgett mixed films of QDs and polymer

With the purpose of organizing QDs into ordered two-dimensional (2D) arrays, we transferred mixed monolayers of polymer PS-MA-BEE and CdSe QDs from the air–water interface onto mica by the LB methodology. To study the effect of the surface composition on the self-assembly process, we have prepared films containing different polymer concentration expressed as polymer mole fraction, X_P: $X_P = n_P/(n_P + n_{QD})$.

In order to study the effect of the surface properties of the Langmuir monolayer precursors of the LB films on the nanoparticles self-assembly, we have transferred Langmuir monolayers at the surface pressure values of 14 mN m^{-1} (the most elastic monolayers) and 30 mN m^{-1} (the least elastic monolayers). Simultaneously, we study the effect of surface composition on the LB film morphology by transferring monolayers with different composition at the two surface pressure values selected.

Fig. 4 shows the AFM and TEM images of some mixed LB films prepared with Langmuir monolayers at the surface pressure value of 14 mN m^{-1} and different surface composition. As can be seen in Fig. 4a, even for films containing low polymer concentration, mixed LB films are denser than the LB films prepared by transferring exclusively QDs onto mica, see Fig. 3a. This can be interpreted by considering that the QDs interact with the most hydrophobic block of the polymer, styrene block [8], remaining adsorbed on the polymer and, the hydrophilic blocks of the polymer favor the interaction with the solid increasing the efficiency of the transfer process. When the polymer concentration increased above $X_P \geq 0.39$ the QDs films break in islands, Fig. 4b–f. Fig. 4f presents high magnification AFM image of these domains, showing that the islands are surrounded by polymer molecules. It is important to note that the morphologies observed by AFM and TEM agree each other and that the domains roughness determined from AFM is independent of the polymer concentration. The average roughness value of 4 nm is compatible with the diameter of the QDs dissolved in chloroform (3.55 ± 0.05 nm).

Our results also demonstrated that even when the QDs composition was too small, the film morphology of PS-MA-BEE/QDs mixed films is different to that corresponding to the polymer PS-MA-BEE. This fact indicates that small concentrations of QDs modify the interactions between the polymer molecules [44–46] distorting the polymer film architecture.

To analyze the effect of the polymer concentration on the QD domain size, the statistical analysis of domain dimensions was carried out. Results are collected in Table 1 and show that the domain size decreases as the polymer mole fraction increases.

We have also transferred PS-MA-BEE/QDs Langmuir films at the surface pressure 30 mN m^{-1} from the air–water interface onto mica by LB. Representative AFM and TEM images of these LB films are collected in Fig. 5. These images suggest two different behaviors depending on the surface composition. In the first one, for LB films of polymer composition below $X_P < 0.93$ shown in Fig. 5a–c, the films are constituted by large QDs domains of roughness 3 nm. The evolution of the domain size with the polymer concentration is similar to that observed for films prepared from Langmuir monolayers at the surface pressure of 14 mN m^{-1}. Thus, when the polymer concentration increases the film evolves to small domains and the distance between domains increases. The second behavior, Fig. 5d–f, was observed for monolayers with high polymer concentration, $X_P \geq 0.93$. At this polymer concentration range the surface pressure isotherms present a plateau and the elasticity values go through a minimum. The AFM and TEM images of these films, Fig. 5d–f shows well-organized hexagonal networks. The order observed in the network formed is highlighted in the FFT diffractogram of the AFM images, where the appearance of several bright spots implies an ordered structure in the LB films [47]. An illustrative example for the LB film prepared at X_P = 0.93 and π = 30 mN m^{-1} is shown in Fig. 5d as inset. On the other hand, it is interesting to note that the roughness of rims around the holes was 4 nm, which is compatible with the diameter of the CdSe QDs dissolved in chloroform (3.55 nm). This fact indicates that the nanoparticles are mainly localized in the rims and do not form 3D aggregates. The hole size of the network cells was measured from the AFM images by taking an average of at least 50 holes per sample and the statistical results are presented in Table 1. The statistical analysis of the holes shows that the hole size in the network decreases with the polymer concentration. This behavior agrees very well with our results in previous work corresponding to mixed LB films of the polymer PMAO and QDs [12]. Finally, when the polymer concentration is further increased above $X_P \geq 0.98$, the QDs concentrations is too low and the film morphology is similar to that corresponding to the polymer film, Fig. 5g. However, the AFM image shows small domains of roughness 4 nm. This roughness is similar to the QDs diameter indicating the presence of some QDs.

The hexagonal network structures in this system are similar to those observed for mixed PMAO/QDs LB films [12], which were interpreted in terms of nucleation and growth of holes dewetting processes [15]. As it was previously mentioned this dewetting mechanism is driven by gravitational effects, consequently, it is easy to understand that this effect predominates in films containing high molecular weight material as the polymer PMAO (40 kDa). However, it is not so evident in the PS-MA-BEE/QDs films because the polymer PS-MA-BEE (2.5 kDa) is too small. To interpret this behavior it is necessary to analyze the balance between gravitatory and capillary forces. Thus, according to the elasticity curves, Fig. 1c, the elasticity goes through a minimum for PS-MA-BEE/QDs monolayers at the surface pressure value of 30 mN m^{-1} and with polymer concentrations above 0.93. Consequently, in these monolayers the capillary waves are quickly damped and the film breaks in domains separated by holes due to gravitatory effects. Conversely, the capillary waves for monolayers with higher elasticity values (π = 14 mN m^{-1} or π = 30 mN m^{-1} and $X_P < 0.93$), do not damp so quickly and they drive the dewetting mechanism. In these situations, the spinodal dewetting mechanism predominates against the growth of holes process leading to circular QDs domains.

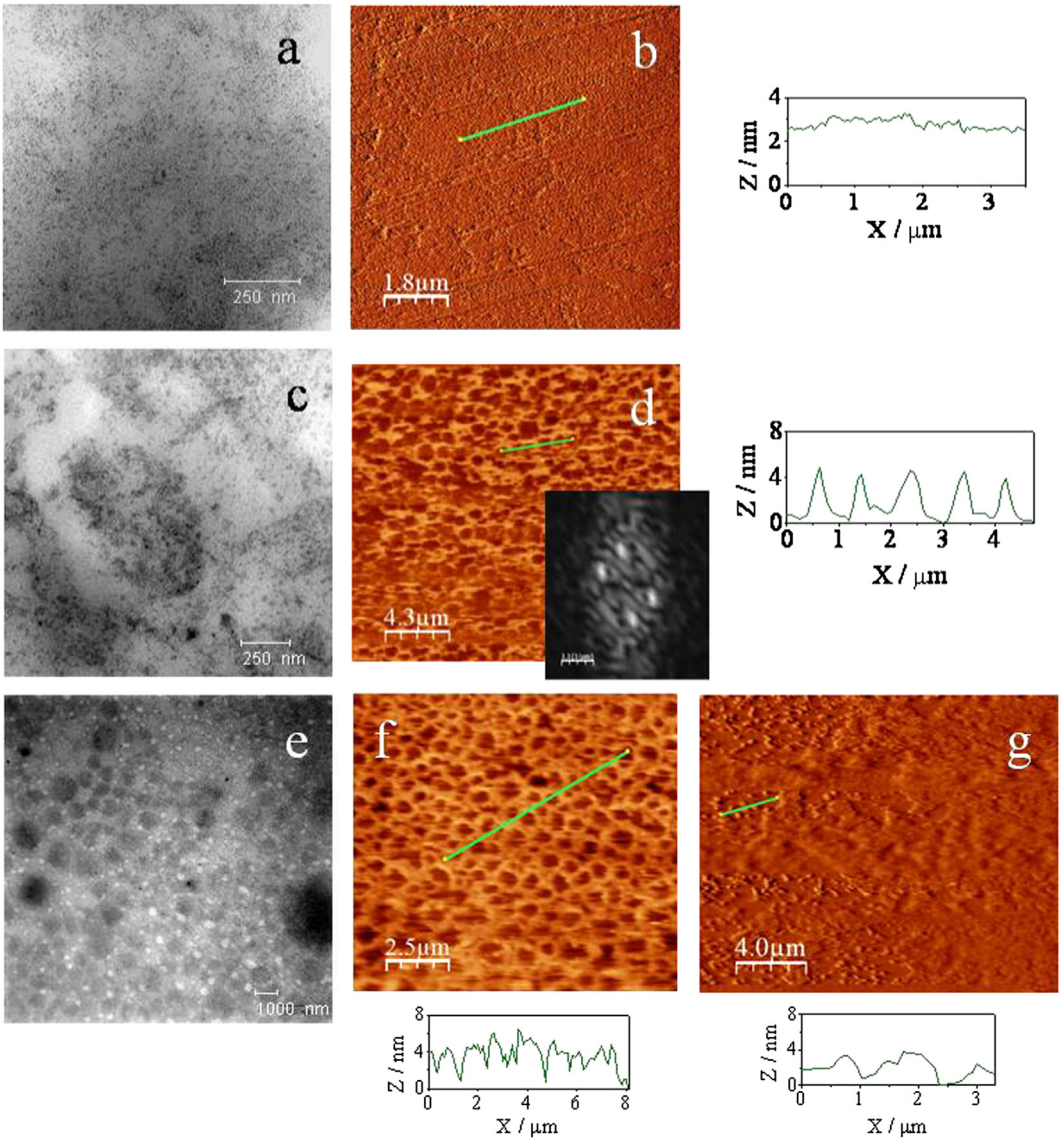

Fig. 5. TEM (a, c, e) and AFM (b, d, f, g) images of mixed QDs/PS-MA-BEE LB films at the surface pressure of 30 mN m^{-1}. The film composition expressed as polymer mole fraction is: 0.25 (a, b); 0.39 (c); 0.93 (d); 0.94 (e, f) and 0.98 (g). The inset in (d) shows the 2D FFT diffractogram calculated with the AFM software.

4. Conclusions

The results obtained in this work demonstrated that the surface state of the block copolymer PS-MA-BEE plays a decisive role on the morphology of the QDs assemblies. Our results show two different film structures depending on film surface properties. Thus, when the Langmuir monolayer precursor of the LB films presents the smallest elasticity value, corresponding to the polymer brush conformation at the surface, the films are composed by hexagonal networks with QDs adsorbed on the rims. Conversely, monolayers with the highest elasticity values give LB films with polymer/QDs domains. The different behaviors were analyzed in terms of distinct dewetting processes, nucleation and growth of holes for the formation of hexagonal networks and spinodal dewetting, for polymer/QDs domains.

The current results together with those obtained previously [12] confirm the ability of the LB methodology to modulate the self-assembly of QDs. Our results demonstrated that it is possible to tune the morphology of the QDs LB films by modifying both the surface composition and surface properties of the Langmuir monolayer precursors of the LB films. This strategy could be presented as a non-template reproducible technique for patterning at the nanoscale.

Acknowledgments

The authors thank financial support from ERDF and MEC (MAT 2010-19727 and MAT 2007-62666) and from Junta de Castilla y León (SA138A08). B.M.G. wishes to thank the European Social Fund and Consejería de Educación de la Junta de Castilla y León for her FPI grant. We also thank to Ultra-Intense Lasers Pulsed Center of Salamanca (CLPU) for the AFM measurements, especially Drs. J.A. Pérez-Hernández and J. Hernández-Toro, and Microscopy Electron Service (Universidad de Salamanca) for the TEM measurements.

References

[1] N. Tomczak, D. Janczewski, M. Han, G.J. Vancso, Prog. Polym. Sci. 34 (2009) 393–430.

[2] R.P. Sear, S.-W. Chung, G. Markovich, W.M. Gelbart, J.R. Heath, Phys. Rev. E 59 (1999) R6255–R6258.
[3] V. Ganesan, J. Polym. Sci. Part B Polym. Phys. 46 (2008) 2666–2671.
[4] M.R. Bockstaller, E.L. Thomas, J. Phys. Chem. B 107 (2003) 10017–10024.
[5] L. Zhao, M. Byun, J. Rzayev, Z. Lin, Macromolecules 42 (2009) 9027–9033.
[6] L. Zhao, M.D. Goodman, N.B. Bowden, Z. Lin, Soft Matter 5 (2009) 4698–4703.
[7] L. Zhao, Z. Lin, Soft Matter 7 (2011) 10520–10535.
[8] S. Zou, R. Hong, T. Emrick, G.C. Walker, Langmuir 23 (2007) 1612–1614.
[9] A.J. Rahedi, J.F. Douglas, F.W. Star, J. Chem. Phys. 128 (2008) 024902.
[10] P. Voudouris, J. Choi, N. Gomopoulos, R. Sainidou, H. Dong, K. Matyjaszewski, M.R. Bockstaller, G. Fytas, ACS Nano 5 (2011) 5746–5754.
[11] M.C. Petty, Langmuir–Blodgett Films: an Introduction, Cambridge University Press, Cambridge, 1996.
[12] T. Alejo, M.D. Merchán, M.M. Velázquez, J.A. Pérez-Hernández, Mater. Chem. Phys. 138 (2013) 286–294.
[13] B. Martín-García, M.M. Velázquez, F. Rossella, V. Bellani, E. Diez, J.L.G. Fierrro, J.A. Pérez-Hernández, J. Hernández-Toro, S. Claramunt, A. Cirera, ChemPhysChem 13 (2012) 3682–3690.
[14] B. Martín-García, M.M. Velázquez, J.A. Pérez-Hernández, J. Hernández-Toro, Langmuir 26 (2010) 14556–14562.
[15] D. Gentili, G. Foschi, F. Valle, M. Cavallini, F. Biscarini, Chem. Soc. Rev. 41 (2012) 4430–4443.
[16] D. Zhao, Q. Huo, J. Feng, B.F. Chmelka, G.D. Stucky, J. Am. Chem. Soc. 120 (1998) 6024–6036.
[17] K. Flodström, V. Alfredsson, Microporous Mesoporous Mater. 59 (2003) 167–176.
[18] P. Kipkemboi, A. Fogden, V. Alfredsson, K. Flodström, Langmuir 17 (2001) 5398–5402.
[19] K. Flodström, V. Alfredsson, N. Källrot, J. Am. Chem. Soc. 125 (2003) 4402–4403.
[20] K. Flodström, H. Wennerström, V. Alfredsson, Langmuir 20 (2004) 680–688.
[21] R. Jones, C.S. Winter, R.H. Tredgold, P. Hodge, A. Hoorfar, Polymer 28 (1987) 1619–1626.
[22] S.J. Collins, N.L. Mary, G. Radhakrishnan, A. Dhathathreyan, J. Chem. Soc. Faraday Trans. 93 (1997) 4021–4023.
[23] J. Listak, I.F. Hakem, H.J. Ryu, S. Rangou, N. Politakos, K. Misichronis, A. Avgeropoulos, M.R. Bockstaller, Macromolecules 42 (2009) 5766–5773.
[24] Y. Lin, A. Boker, J. He, K. Sill, H.Q. Xiang, C. Abetz, X.F. Li, J. Wang, T. Emrick, S. Long, Q. Wang, A. Balazs, T.P. Russell, Nature 434 (2005) 55–59.
[25] J.J. Chiu, B.J. Kim, E.J. Kramer, D.J. Pine, J. Am. Chem. Soc. 127 (2005) 5036–5037.
[26] W.W. Yu, X. Peng, Angew. Chem. Int. Ed. Engl. 41 (2002) 2368–2371.
[27] J. Jasieniak, L. Smith, J. van Embden, P. Mulvaney, M. Califano, J. Phys. Chem. C 113 (2009) 19468–19474.
[28] I. Horcas, R. Fernández, J.M. Gómez-Rodríguez, J. Colchero, J. Gómez-Herrero, A.M. Baro, Rev. Sci. Instrum. 78 (2007) 013705.
[29] K.M. Gattás-Asfura, C.A. Constantine, M.J. Lynn, D.A. Thimann, X. Ji, R.M. Leblanc, J. Am. Chem. Soc. 127 (2005) 14640.
[30] D. López-Díaz, M.M. Velázquez, Eur. Phys. J. E 26 (2008) 417–425.
[31] A.M. Gonçalves da Silva, M.I. Viseu, C.S. Campos, T. Rechina, Thin Solid Films 320 (1998) 236–240.
[32] R.B. Cheyne, M.G. Moffitt, Langmuir 22 (2006) 8387–8396.
[33] I.I. Perepichka, K. Borozenko, A. Badia, C.G. Bazuin, J. Am. Chem. Soc. 133 (2011) 19702–19705.
[34] C.P. Glagola, L.M. Miceli, M.A. Milchak, E.H. Halle, J.L. Logan, Langmuir 28 (2012) 5048–5058.
[35] B.A. Noskov, S.-Y. Lin, G. Loglio, R.G. Rubio, R. Miller, Langmuir 22 (2006) 2647–2652.
[36] A.M. Diez-Pascual, F. Monroy, F. Ortega, R.G. Rubio, R. Miller, B.A. Noskov, Langmuir 23 (2007) 3802–3808.
[37] Y.-L. Lee, Z.-C. Du, W.-X. Lin, Y.-M. Yang, J. Colloid Interface Sci. 296 (2006) 233–241.
[38] S. Gupta, N. Singh, M. Sastry, R. Kakkar, R. Pasricha, Thin Solid Films 519 (2010) 1072–1077.
[39] A. Gole, N.R. Jana, S.T. Selvan, J.Y. Ying, Langmuir 24 (2008) 8181.
[40] N.J. Suematsu, Y. Ogaw, Y. Yamamoto, T. Yamaguchi, J. Colloid Interface Sci. 310 (2007) 648–652.
[41] H. Yabu, M. Shimomura, Adv. Funct. Mater. 15 (2005) 575–581.
[42] O. Karthaus, S. Mikami, Y. Hashimoto, J. Colloid Interface Sci. 301 (2006) 703–705.
[43] J. Lucassen, Trans. Faraday Soc. 64 (1968) 2221–2229.
[44] S.W. Sides, B.J. Kim, E.J. Kramer, G.H. Fredrickson, Phys. Rev. Lett. 96 (2006) 250601.
[45] F.D.A.A. Reis, Macromolecules 41 (2008) 8932–8937.
[46] K.M. Langner, G.J.A. Sevink, Soft Matter 8 (2012) 5102–5118.
[47] J.P.K. Peltonen, P. He, J.B. Rosenholm, J. Am. Chem. Soc. 114 (1992) 7637–7642.